SCIENCE CHINA
Earth Sciences

•ARTICLE•

July 2024 Vol.67 No.7: 2084–2102
https://doi.org/10.1007/s11430-023-1341-4

Characteristics of super drought in Southwest China and the associated compounding effect of multiscalar anomalies

Lin WANG[1,2], Wen CHEN[3*], Gang HAUNG[4], Ting WANG[5*], Qiulin WANG[6], Xiaoyun SU[4], Zixuan REN[7], Chakrit CHOTAMONSAK[8,9], Atsamon LIMSAKUL[10] & Kritanai TORSRI[11]

[1] *CAS Key Laboratory of Regional Climate-Environment for Temperate East Asia, Institute of Atmospheric Physics, Chinese Academy of Sciences, Beijing 100029, China;*
[2] *Heavy Rain and Drought-Flood Disasters in Plateau and Basin Key Laboratory of Sichuan Province, Chengdu 610072, China;*
[3] *Department of Atmospheric Science, Yunnan University, Kunming 650500, China;*
[4] *State Key Laboratory of Numerical Modeling for Atmospheric Sciences and Geophysical Fluid Dynamics, Institute of Atmospheric Physics, Chinese Academy of Sciences, Beijing 100029, China;*
[5] *Carbon Neutrality Research Center, Institute of Atmospheric Physics, Chinese Academy of Sciences, Beijing 100029, China;*
[6] *Hangzhou Meteorological Bureau, Hangzhou 310051, China;*
[7] *Center for Monsoon System Research, Institute of Atmospheric Physics, Chinese Academy of Sciences, Beijing 100029, China;*
[8] *Department of Geography, Faculty of Social Sciences, Chiang Mai University, Chiang Mai 50200, Thailand;*
[9] *Environmental Science Research Center, Faculty of Science, Chiang Mai University, Chiang Mai 50200, Thailand;*
[10] *Climate Change and Environmental Research Center, Technopolis, Klong 5, Klong Luang, Pathumthani 12120, Thailand;*
[11] *Hydro-Informatics Innovation Division, Hydro-Informatics Institute, Ministry of Higher Education, Science, Research and Innovation, Bangkok 10900, Thailand*

Received December 12, 2023; revised May 7, 2024; accepted May 17, 2024; published online June 6, 2024

Abstract In recent decades, Southwest China (SWC) has suffered from frequent super droughts, leading to severe economic losses and ecological degradation. This study investigates the characteristics of super droughts in SWC during 1961–2022, reveals the compounding effect of multiscalar anomalies, and explores the plausible atmospheric circulation mechanisms responsible. The nature of super drought is a compound drought caused by the superposition of extreme drought events across multiple time scales. By contrasting the typical drought cases in 2006 and 2022, the decisive role of multiscalar drought compounding is confirmed. Based on the Comprehensive Multiscalar Index (CMI), multiple super drought events in SWC were identified to be temporally clustered during 2006–2014. Among them, the decadal background of enhanced evaporation and precipitation deficit at long time scales is a necessary condition for shaping the overall pattern of super droughts, while the precipitation and evaporation anomalies at short time scales trigger the outbreak of super droughts, determining the exact timing of occurrence. These events include August–September 2006, November 2009 to May 2010, July–October 2011, April–May 2012, January–April 2013, etc. Statistical results suggest that the contribution of superposed precipitation anomalies to super drought is 2.4 times that of evaporation. As regards the circulation mechanisms affecting multiscalar precipitation, the anomalous spatial patterns at short-term and long-term scales are similar, featuring the cyclonic circulation over the South China Sea and the northeasterly wind anomalies together with the subsidence center over SWC. During 2006–2014, the possible causes for the cross-seasonal persistent precipitation reduction in SWC are the extreme negative phase of the Pacific Decadal Oscillation (PDO) in the North Pacific as well as the pronounced warming of the warm pool in the western Pacific. The key dynamic processes are outlined as follows. On the one hand, the negative PDO phase generates anomalous anticyclonic circulation in the North Pacific, with the northeasterly winds on its southwest flank extending to Southeast Asia, hindering moisture transport into SWC. On the other hand, the warming of the warm pool excites anomalous cyclonic circulation to its northwest, also giving rise to northeasterly wind anomalies over SWC. Meanwhile, the ascending motion over the warm pool region diverges at upper levels with outflows

* Correspondence authors: Wen CHEN (chenwen-dq@ynu.edu.cn), Ting WANG (wangting@mail.iap.ac.cn)

converging aloft over SWC, which further induces compensating downward motion there. The combined effect of the above two remote forcings establishes a climatic background state unfavorable for precipitation over SWC at long time scales, thus constituting a crucial prerequisite for the superimposition of short-term precipitation anomalies to develop into super droughts.

Keywords Super drought, Multiscalar, Compounding effect, Mechanism analysis, Southwest China

Citation: Wang L, Chen W, Haung G, Wang T, Wang Q, Su X, Ren Z, Chotamonsak C, Limsakul A, Torsri K. 2024. Characteristics of super drought in Southwest China and the associated compounding effect of multiscalar anomalies. Science China Earth Sciences, 67(7): 2084–2102, https://doi.org/10.1007/s11430-023-1341-4

1. Introduction

Southwest China (SWC) includes Sichuan, Chongqing, Guizhou, Yunnan, and Guangxi, accounting for one-sixth of the country's population and 16% of the national grain production. This region serves as the "source of rivers" for China and even South and Southeast Asia, as it is the origin and upper reaches of some important domestic and international rivers such as the Yangtze River, Pearl River, Lancang River, and Yarlung Zangbo River. Consequently, SWC possesses 46% of China's water resources. Figure 1 illustrates the geographical location and topography of SWC.

Despite being a humid region, however, SWC has been hit by frequent extreme drought events in recent years. In 2006, a severe high-temperature and drought disaster occurred in Sichuan and Chongqing, causing drinking water shortages in both areas, with the drought-affected area of crops exceeding 3.2 million hectares and a grain yield reduction of about 5 million tons (Li et al., 2011). Just three years later, from the autumn of 2009 to the spring of 2010, Yunnan, Guizhou, Sichuan, and other regions in SWC experienced a prolonged and severe drought lasting nearly eight months. This extreme event not only caused widespread crop failures in the affected areas but also led to difficulties in living water use for about 25 million people, eventually resulting in enormous economic losses (Huang et al., 2012). The summer of 2011 saw SWC facing yet another extreme drought, with a total of 38.763 million people affected, 10.398 million people and 5.377 million livestock facing temporary drinking water shortages, and 3.344 million hectares of crops impacted, of which 550,000 hectares yielded no harvest. This drought event caused a direct economic loss of approximately 21.3 billion yuan (Duan et al., 2011). Furthermore, from January to April 2013, some parts of SWC once again encountered another continuous severe drought, affecting 29.387 million people across the four provinces/municipalities of Yunnan, Sichuan, Guizhou, and Chongqing, with 72.59 million people suffering from drinking water difficulties and 43.48 million people requiring living assistance (Hu et al., 2015).

The geographical location of SWC is unique, as it is the confluence area of the South Asian monsoon and the East Asian monsoon, which makes its weather and climate patterns, as well as their underlying causes, highly complex (Chen et al., 2023, 2024; Zhang et al., 2024). Climatological studies on drought in SWC can be generally categorized into three types: analyses of the historical evolution, examinations of the large-scale circulation patterns as well as physical mechanisms, and future scenario projections. While there is a large body of relevant research, it is not possible to review all of them due to space constraints; instead, readers can refer to the review article by Wang et al. (2015a) on the progress of drought research in SWC. Moreover, Zhang et al. (2024) comprehensively reviewed and summarized the latest research progress on various aspects of droughts, including drought formation mechanisms, prediction theories and methods, as well as drought disaster risk characteristics. In this regard, we mainly sketch some recent achievements pertaining to drought research in SWC and provide representative examples for the above three research directions.

Concerning the characteristics of drought evolution in SWC, Wang et al. (2022) investigated the characteristics of extreme drought in East Asia over the past 60 years based on a qualitative comprehensive multiscalar indicator. They highlighted that the frequency of extreme drought has increased significantly in the last decade, with two main hotspot areas in China: the transitional climate zone in the north and SWC. In addition to the recent period, Wang and Chen (2012) noted that SWC also experienced extremely severe droughts around 1940 based on records spanning nearly a century. Liu et al. (2017) examined the spatial discrepancies in the climatic change of drought in SWC and found that the spatial variability of drought duration, intensity, and joint return period has decreased significantly, indicating that droughts have become more widespread rather than localized in certain sub-regions.

When it comes to investigating the large-scale circulation background and causes of drought in SWC, studies have mainly concentrated on the analysis of extreme cases as well as the causes of interannual and interdecadal variability. In terms of extreme case analysis, Zhang (2020) compared and analyzed moisture sources and their changes during extreme summer droughts in 2006 and 2011, and found that the 2006 drought was mainly caused by reduced moisture transport from the Indian monsoon and westerlies, while the 2011 drought was a result of the combined reduction in moisture transport from the Indian monsoon, westerlies, and East Asian summer monsoon. Sun et al. (2019) examined extreme

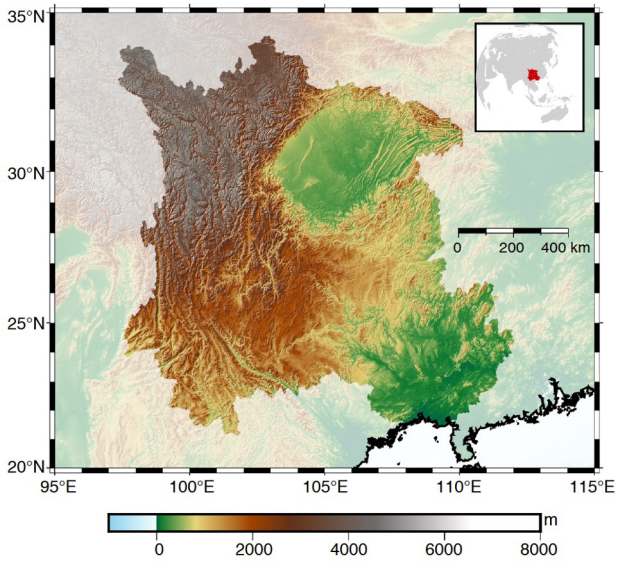

Figure 1 The geographical location of SWC (upper right inset) and its topographic elevation map (main map).

drought events from 2009 to 2011 and suggested that the drought intensity in 2009 and 2011 was primarily attributed to decreased precipitation, whereas the impacts of precipitation and evaporation were comparable in 2010. Apart from the influence of internal variability in the climate system, certain studies have also addressed the contribution of external forcings from human activities, such as Wang et al. (2021). On the interannual time scale, Jiang et al. (2017) pointed out that summer precipitation in SWC has two dominant modes of interannual variability. The first mode features a consistent variation across the entire region except for central Sichuan, while the second mode exhibits an opposite variation between the northern and southern parts of the region. They further indicated that the strength of convective activity over the Philippine Sea is closely related to the first mode, whereas the convective activity over the western Maritime Continent influences the formation of the second mode. For autumn precipitation, Wang et al. (2015b) pointed out that the sea surface temperature (SST) in the tropical Northwest Pacific (NWP) plays an important role. The key dynamic process is that warm SST anomalies in the NWP can trigger anomalous cyclonic circulation over the South China Sea, which weakens moisture transport towards SWC, thereby suppressing precipitation in this region. Besides the impact of tropical systems, Hao et al. (2022) noted that the summer North Atlantic Oscillation (NAO) also plays a crucial role in modulating autumn precipitation in SWC, with the negative phase of the NAO resulting in drier conditions in SWC in the subsequent November. The primary dynamic processes involve two wave trains along the subtropical jet and great circle path. Moreover, Wu et al. (2023) and Tao et al. (2023) examined the interannual variations and causes of the onset and cessation timings of the rainy season in SWC. On the interdecadal scale, Wang et al. (2018) observed that the autumn climate in SWC underwent an interdecadal transition from "wet" to "dry" in 1994. Based on statistical diagnostic methods, the Indo-Pacific warm pool was identified as a key region in driving the interdecadal-scale drought in SWC. The Indo-Pacific warm pool also experienced an interdecadal shift in 1994, transitioning from cold to warm SST, which coincided exactly with the timing of the interdecadal wet-to-dry shift in SWC. The main dynamic processes include the cyclonic circulation anomaly over the South China Sea, the southeasterly wind anomaly south of the Tibetan Plateau, the eastward displacement of the water vapor transport path over the equatorial Indian Ocean, and the compensating sinking airflow over SWC. Jia et al. (2021) further suggested that the interdecadal variation of SST in the North Atlantic, which triggers atmospheric teleconnections, also has a remarkable impact. Additionally, Tan et al. (2017) analyzed the interdecadal variation of winter precipitation, highlighting that winter precipitation in SWC has been persistently deficient since 2000. This interdecadal change is related to the negative phase of the Arctic Oscillation (AO) and the frequent occurrence of central Pacific El Niño events. Dong et al. (2023) examined the interdecadal variation of summer precipitation, emphasizing that the primary SST forcings include the Bay of Bengal, the western Pacific warm pool, and the western North Pacific. Apart from the influence of internal variability in the climate system, Huo et al. (2021) indicated that the direct and indirect effects, and induced circulation changes caused by increased anthropogenic aerosols, have contributed to a decrease in autumn precipitation in SWC.

Regarding the future scenario projections of drought in SWC, Wang et al. (2014) assessed the future evolution trend of drought in SWC based on CMIP5 data. In the early 21st century, the projected precipitation changes show spatial inconsistency, with decreases in most areas but increases in the northwestern mountainous regions. However, in the mid-to-late 21st century, entire SWC region is expected to undergo increased precipitation, primarily due to the enhanced southwesterly moisture transport from the Bay of Bengal. In parallel, evaporation is expected to increase gradually, mainly driven by the increase in net radiation and temperature, as well as the decrease in relative humidity. Although both precipitation and evaporation are projected to increase, the rate of evaporation increase exceeds that of precipitation, implying that the mitigating effect of precipitation on drought is entirely offset by the strong evaporation. Concurrently, the occurrence probabilities of both extreme drought and wet events are projected to increase significantly, leading to a more extreme climate in SWC in the future. In addition, Leng et al. (2020) indicated that the risk of drought in SWC is higher in autumn, winter, and spring in

the future.

These studies are highly important for understanding the changes and causes of drought in SWC. Nevertheless, there are still some shortcomings. Previous studies have mostly concentrated on investigating the characteristics and causes of drought at a single time scale, such as anomalies during the period of extreme events, while less attention has been placed on the compounding effect at different time scales. In fact, the latest research findings suggest that high-impact droughts are essentially compound drought events caused by the superposition of extreme drought events across multiple time scales, known as super droughts (Wang et al., 2023), and SWC is no exception (Wang et al., 2016). Recently, some studies have begun to recognize the differences in the variation patterns and formation mechanisms of droughts at different time scales (Zhang et al., 2020; Zhang et al., 2022). Hence, building upon previous studies, it is imperative to conduct a comprehensive and systematic analysis of the characteristics of super droughts in SWC, aiming to unveil the compounding effects of droughts at different time scales and their associated atmospheric circulation driving factors.

2. Data

The precipitation and potential evapotranspiration (PET) data are obtained from the latest CRU TS4.07 monthly gridded dataset released by the University of East Anglia, UK (Harris et al., 2020). This dataset provides monthly precipitation and PET data at a 0.5° × 0.5° resolution, covering the global land from 1901 to 2022. The PET is estimated based on the Penman-Monteith scheme. To ensure data quality, we select data from 1961 onward for analysis. Additionally, we employ actual evaporation data as supplementary evidence, which is retrieved from the latest version (v3.7b) of the Global Land Evaporation Amsterdam Model (GLEAM) jointly developed by the University of Amsterdam and Ghent University. The GLEAM dataset has a spatial resolution of 0.25° and spans from 2003 to 2022 (Miralles et al., 2011; Martens et al., 2017). The v3.7b product relies solely on satellite data to compute evaporation using the Priestley–Taylor model, with input data including radiation flux, soil moisture, precipitation, temperature, vegetation optical thickness, and snow water equivalent. We extract the regionally averaged time series of deseasonalized monthly PET and actual evaporation anomalies in SWC from 2003 to 2022, and find their correlation coefficient to be 0.43, which is statistically significant at the 0.0001 level. This suggests that, as a subtropical humid region, the variation of actual evaporation in SWC is predominantly governed by PET. In the following discussion, we mostly use the term "evaporation", but we will explicitly specify "PET" when it comes to quantitative analysis.

To quantitatively identify super droughts, the CMI is obtained from the super drought online product platform https://superdrought.com. This product is calculated based on the CRU TS4.07 data and offers monthly gridded CMI values at a 0.5° resolution over global land from 1961 to 2022. In addition, the Standardized Precipitation Evapotranspiration Index (SPEI) is calculated for time scales of 3, 6, 12, 24, and 48 months using the CRU TS4.07 data (Vicente-Serrano et al., 2010). When processing the data to reflect the overall features of regional drought, there are usually two averaging methods: one is to directly average the gridded index values, which is the most common approach; the other is to first average the original precipitation and PET values within the region, and then calculate the regional index based on the averaged values. It is worth mentioning that the specific values obtained from these two methods differ, with the direct averaging of gridded indices tending to underestimate, but their temporal patterns are consistent and do not affect the assessment of drought variability. Therefore, when investigating drought conditions in SWC region, this study takes into account the second calculation method as well.

To corroborate the results depending on the CMI, we also utilize the terrestrial total water storage data derived from the GRACE satellite gravity observations published by the Center for Space Research (CSR) at the University of Texas (Tapley et al., 2019). The terrestrial total water storage data, expressed in equivalent water height (unit: cm), encompass surface water, soil water, runoff, and groundwater. The data version used in this study is the latest RL06.2 Mascon product, which extends from April 2002 to the present, with a spatial resolution of 0.5°×0.5° and a temporal resolution of 1 month (Save et al., 2016). Mascon, short for mass concentration, represents a new generation of GRACE products. Its greatest advantage lies in its readiness for use without requiring any post-processing, whereas the traditional spherical harmonic coefficient solution requires post-processing steps such as low-degree coefficient replacement and supplementation, as well as de-striping (Zhang and Sun, 2022).

The atmospheric circulation data used in this study are from the fifth-generation global atmospheric reanalysis monthly dataset ERA5 released by the European Centre for Medium-Range Weather Forecasts (ECMWF) (Hersbach et al., 2020). ERA5 provides global atmospheric, surface, and oceanic parameters on a monthly grid from 1940 onwards, with a horizontal resolution of 0.25°×0.25°. The data used in this study cover the period from 1961 to 2022 and comprise variables such as total column water vapor flux, wind field, and vertical velocity field. The SST data are acquired from the Extended Reconstructed SST (ERSST) version 5 dataset provided by NOAA/NCEI, which is a monthly average SST reconstruction from 1854 to the present, with a spatial resolution of 2°×2° (Huang et al., 2017). The analysis period for the ERSST dataset is also set as 1961–2022. In addition,

the Pacific Decadal Oscillation (PDO) index is obtained from NOAA/NCEI and can be downloaded from https://www.ncei.noaa.gov/access/monitoring/pdo/.

3. Methods

3.1 The concept of super drought and the Comprehensive Multiscalar Index (CMI)

First, we briefly introduce the background and the need for proposing the concept of super drought. Unlike research on extreme precipitation and extreme temperature, the distinctive feature of drought is its multiscalar nature, which is a critical concept in drought studies. This concept differs from the temporal scale concepts commonly used in climatological research, such as interannual and interdecadal variations. In fact, it refers to the multi-type characteristics of drought, i.e., water resources are stored in various forms in nature, including precipitation, soil moisture, groundwater, river water, lake water, and reservoir water, each of which responds to water deficits at different time scales. By definition, the time scale of drought refers to a temporal window extending backward from the current month, which is considered when assessing the dry/wet conditions of that particular month. The cumulative water balance within this time window is compared with the multi-year average of the same period to ultimately determine the dry and wet conditions of that month. For instance, the 3-month time scale assesses the cumulative water balance of the previous 2 months and the current month, while the 6-month time scale considers the cumulative water balance of the previous 5 months and the current month. Commonly, drought indices are calculated at time scales of 3, 6, 12, 24, and 48 months. As the length of the time scale window increases, drought can be broadly divided into meteorological drought, agricultural drought, and hydrological drought, and the changes in the drought index tend to become more gradual. Hence, for the same geographical region and the same time point, if different time scales (i.e., different types of drought) are considered, the dry and wet states can be entirely different. For example, a 3-month precipitation deficit may result in meteorological drought and agricultural drought caused by reduced soil moisture content, but it has a relatively minor impact on the hydrological system, implying that the river flow and reservoir water storage remain in a normal or even wet state. Conversely, a long-term (several quarters or years) precipitation deficit may lead to severe hydrological drought, but a strong precipitation event during this period may cause the soil to be in a wet state, while the hydrological system remains in a drought state. This apparent "asynchronous" state poses significant challenges in determining the overall extreme drought conditions of a region.

It is exactly due to the potential occurrence of "asynchronous" states among different water resource components that the concept of "super drought" was introduced (Wang et al., 2023). Super drought refers to the simultaneous occurrence of extreme droughts at multiple time scales, which can be regarded as the superposition of diverse types of extreme droughts, constituting a type of compound extreme drought event. If an extreme drought occurs only at a specific time scale, its destructive impact may be limited; however, when extreme droughts of different time scales coincide, it will lead to extensive and severe impacts on the water resource system. The physical significance of super drought lies in a serious shortage of total available water resources, rather than a lack of water in a certain component. Moreover, it also reveals that the essential feature behind extreme drought events is not that a certain indicator reaches a historical low, but rather whether droughts at different time scales undergo compounding, which is the key to distinguishing between general droughts and high-impact droughts.

To quantitatively characterize super drought, Wang et al. (2023) took into account the nonlinear characteristics and complex interactions among different time scales of drought and developed a complete algorithm framework based on vine copula to ultimately construct the Comprehensive Multiscalar Index (CMI). The CMI probabilistically integrates drought information at different time scales by determining the anomaly value through the entire measure space, thus reflecting the comprehensive state of multiscalar drought. Through validation at regional and global scales, it has been demonstrated that the CMI can effectively capture the comprehensive characteristics of multiscalar drought and significantly outperforms traditional drought indices in reflecting overall water resource changes and overall extremity. Thus, the CMI has proven to be a valuable tool for monitoring and identifying super droughts. Moreover, the methodology for constructing the CMI exhibits strong versatility and adaptability, without specific requirements for the input data. Theoretically, various types of drought-related variables, such as precipitation, soil moisture, and groundwater, can all be used as input data sources to flexibly construct the vine copula model.

The following briefly describes the calculation steps of the CMI, with specific methods referred to Wang et al. (2023). The first step involves data preparation and preprocessing. Based on precipitation and PET data, the cumulative water balance at different time scales k is calculated as follows: $D_n^k = \sum_{i=0}^{k-1}(\mathrm{PET}_{n-i} - P_{n-i}), n \geqslant k$, where n is the month and k is the time scale. Then, the marginal distribution of D_n^k is converted into a uniform distribution in the [0, 1] interval through the empirical probability integral transformation method. The second step involves the construction and goodness-of-fit test of vine copula model. First, the Kendall

rank correlation coefficients between each pair of variables at different scales are computed, and according to the maximum spanning tree algorithm, the structure that maximizes the absolute sum of the Kendall rank correlation coefficients is selected as the regular vine structure. Next, the Akaike Information Criterion (AIC) is used to determine the type of bivariate copula function corresponding to each connection edge, and the parameters are estimated using the maximum likelihood method. The candidate bivariate copulas include the independence copula, elliptical copula family (2 types), and Archimedean copula family (8 types), among which the Archimedean copula family (except Frank copula) can be rotated by 90°, 180°, and 270°. Finally, the Rosenblatt probability integral transformation method is applied to test the goodness-of-fit of the vine copula model. The third step is the generation of the CMI. First, the distribution function of the vine copula is obtained through Monte Carlo simulation. Then, the Kendall function is utilized to convert the copula measure to the Kendall measure, which is subsequently standardized using the standard normal distribution. Finally, it is multiplied by −1 to derive the CMI for evaluating the comprehensive drought risk and identifying super droughts.

In this study, we chose five time scales: 3, 6, 12, 24, and 48 months, to construct the CMI. The selection of these time scales considers both the representativeness of multiple time scales from short-term to long-term and the balance of computational efficiency (Wang et al., 2023). It is important to note that during the construction process of the vine copula, we adopted the "maximum absolute value of the Kendall rank correlation coefficient" as the criterion, which is primarily used to determine the structure of the vine, i.e., deciding which two variables preferentially couple rather than ultimately selecting only 2 out of the 5 time scales for the CMI calculation. In fact, due to the highest correlation between adjacent time scales, the resulting vine structure is sequentially 3–6–12–24–48 months, which happens to belong to a special class of copula called the D-vine. Through global-scale validation, Wang et al. (2023) found that for the multiscalar drought problem, this D-vine structure is the optimal choice in most cases. In summary, the calculation of the CMI takes into account the contributions of all 5 typical time scales, and the Vine Copula-based computational framework can effectively capture the complex interrelationships and nonlinear characteristics among different time scales.

3.2 Online platform for super drought products

To promote the application of research findings and facilitate access to super drought-related information for researchers and decision-makers, an online platform for super drought products has been established. The platform, available at https://superdrought.com, publishes monthly global super drought monitoring information and historical datasets. The monitoring product updates the CMI on a monthly basis, providing the latest information on the current situation. Users can interactively view the values of any region and keep track of the occurrence of super droughts. The historical database contains monthly CMI datasets covering the global land from 1961 to 2022, provided in 0.5°×0.5° gridded netCDF format. Based on updates to the source data, the content of the database will be irregularly updated, and users can extract and analyze the super drought characteristics for periods and regions of interest. The platform content and functionality will be continuously updated and improved.

3.3 Multiscalar processing of driving factors

The compounding effect of multiscalar droughts is a crucial mechanism for the formation of super droughts. Therefore, it is necessary to perform multiscalar processing on the key variables driving drought, including precipitation, evaporation, atmospheric circulation and SST that influence the climate system, to reveal the mechanisms underlying the superposition of droughts across multiple time scales. Since the precipitation and PET variables can accumulate, we calculate the cumulative values at different time scales, which is consistent with the method of calculating the cumulative water balance at different time scales in the CMI calculation process. Specifically, for a given moment n, we define $Q_n^k = \sum_{i=0}^{k-1} Q_{n-i}, n \geqslant k$, where k represents the time scale and Q_n^k represents the cumulative precipitation or PET from the current month n to the previous $k-1$ months. For variables related to atmospheric circulation and SST, since quantities such as wind speed are not suitable for direct accumulation, the method of taking average values with different sliding window periods is adopted to represent the atmospheric and oceanic driving effects at different time scales. Specifically, for a given moment n, we define $S_n^k = \frac{1}{k}\sum_{i=0}^{k-1} S_{n-i}, n \geqslant k$, where S represents the atmospheric or oceanic variable and S_n^k represents the average value of the variable from the current month n to the previous $k-1$ months. Then, for each calendar month, the anomalies of these cumulative values or cumulative averages are calculated relative to the climatic average of that specific month.

4. Characteristics of super drought in SWC and the compounding of multiscalar droughts

4.1 Characteristics of super drought based on the CMI

Figure 2 presents the changes in the monthly precipitation

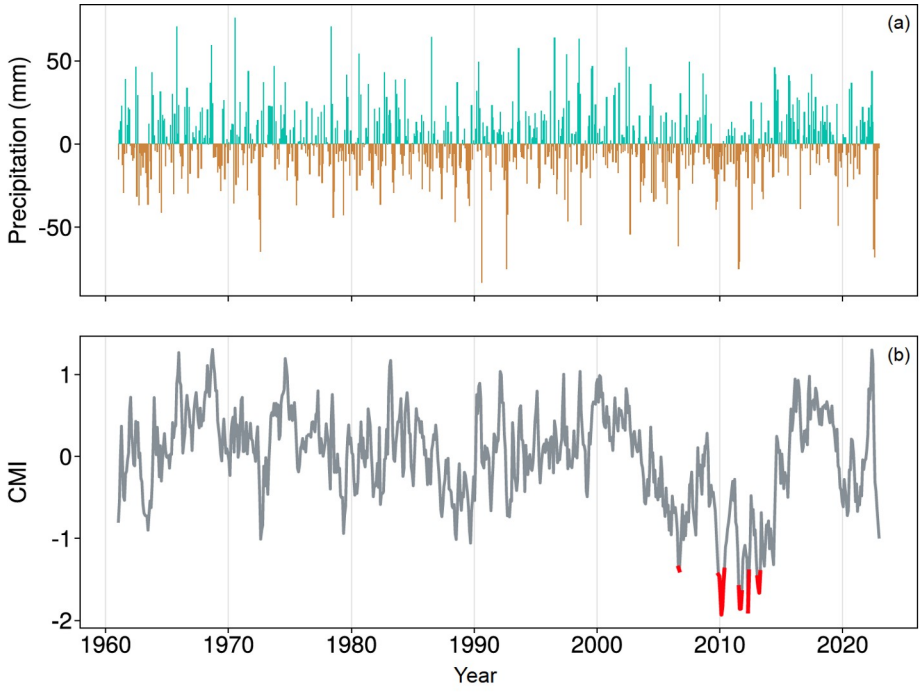

Figure 2 Time series of precipitation anomalies (a) and CMI (b) averaged over SWC from 1961 to 2022. In (b), CMI values less than −1.3 are marked in red.

anomalies and CMI averaged over SWC from 1961 to 2022. As shown in Figure 2a, precipitation in SWC exhibits significant month-to-month variability, with a standard deviation of 20.5 mm, and there is no notable increasing or decreasing trend over the past 60 years. From the perspective of precipitation anomalies alone, it is entirely impossible to distinguish extreme drought events. For example, during the widespread and prolonged drought from autumn 2009 to spring 2010, the average precipitation anomaly in SWC was only −10.5 mm, which is half of the standard deviation. On the other hand, the top two ranked negative precipitation anomalies occurred in August 1990 and August 1992, with values of −83 mm and −75 mm, respectively, but no extreme drought events took place during these two months. In addition to using precipitation anomalies, any single-time-scale SPEI also has similar limitations in identifying extreme drought events, as explained in Appendix A (https://link.springer.com). Thus, the traditional approach fails to characterize extreme drought events. The reason is that disastrous drought events are typically caused by the superposition of extreme drought events at multiple time scales, or equivalently, multiple types of droughts (Wang et al., 2023; Zhang et al., 2020). Traditional indices, however, do not provide a comprehensive assessment of drought, as they only reflect the drought characteristics of a single time scale or a single type rather than the overall situation of water resources. This can lead to erroneous judgments.

The CMI integrates multiscalar drought information and is used to quantify the overall severity of drought. When it reaches a certain threshold, it can capture the true extreme drought state. Figure 2b depicts the variation of the CMI averaged over SWC from 1961 to 2022. Prior to 2000, the CMI fluctuated around 0, and its lowest value rarely exceeded −1, suggesting that the overall water resources in SWC remained relatively stable. However, since the beginning of the 21st century, the CMI has shown a continuous downward trend, reaching its historical lowest value around 2010, after which the CMI gradually recovered to normal levels. Using −1.3 as the threshold for determining super drought events, the results indicate that multiple super drought events occurred frequently between 2006 and 2014, including August–September 2006, November 2009 to May 2010, July–October 2011, April–May 2012, and January–April 2013. The identified super droughts are highly consistent with the severe socioeconomic damage events that occurred during that period, fully justifying that the CMI is an effective tool for determining the overall severity of regional drought and identifying super drought events.

4.2 The compounding effect of multiscalar droughts

Next, we continue to analyze the synergistic effect of multiscalar water resource anomalies during these super drought processes. Figure 3 presents the SPEI values at 3-, 6-, 12-, 24-, and 48-month time scales as well as the CMI values averaged over SWC from 1963 to 2022. The results indicate

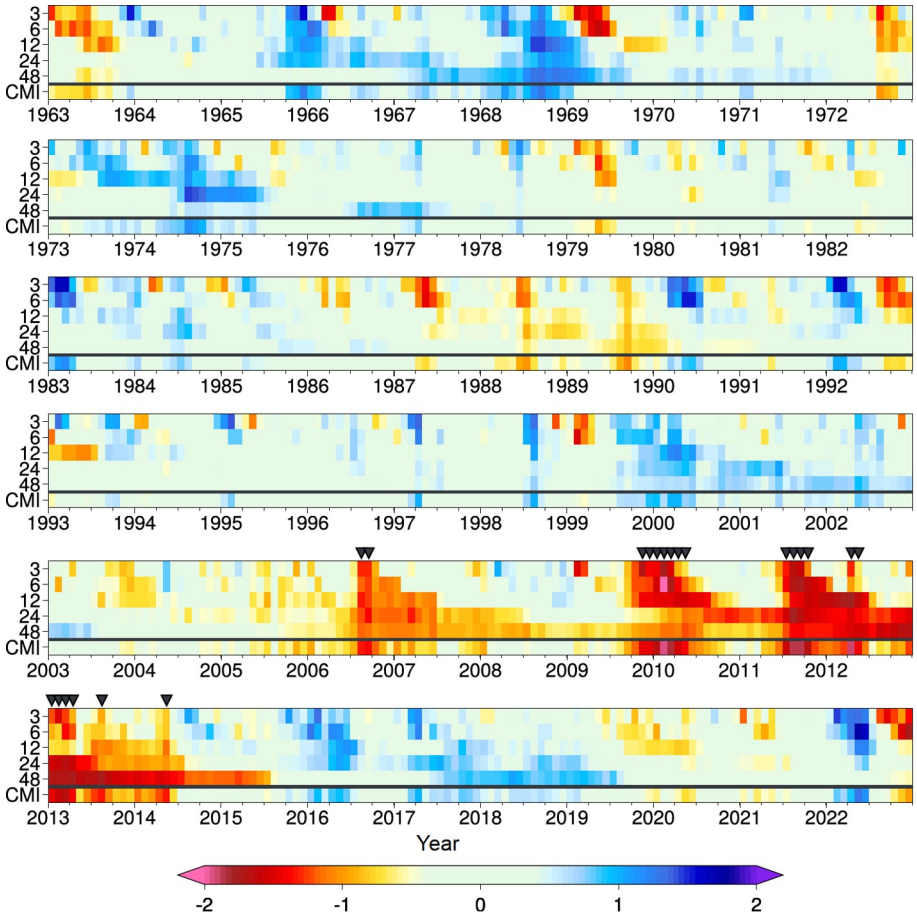

Figure 3 SPEI values at 3-, 6-, 12-, 24-, and 48-month time scales as well as CMI values averaged over SWC from 1963 to 2022. The *y*-axis labels 3, 6, 12, 24, and 48 represent the corresponding SPEI time scales, while the label CMI represents the CMI.

that during the super drought processes, the SPEI values at different scales all exhibit abnormally negative values below the normal level, representing shortages in various types of water resource components concurrently. For instance, during the super drought period from November 2009 to May 2010, the SPEI values at the 6- and 12-month time scales reached extreme drought levels below −2, and the SPEI values at the 3-, 24-, and 48-month time scales were also below −1. This suggests that meteorological, agricultural, and hydrological droughts occurred simultaneously, leading to a severe reduction in overall water resources in the region, constituting a super drought state. Correspondingly, the CMI shows extreme negative values below −2. It is necessary to clarify that the values mentioned here are the SPEI and CMI values calculated after first averaging the original variables over the region.

To further demonstrate the crucial role of multiscalar drought compounding, we compare and analyze the differences between the two typical drought events that occurred in August 2006 and August 2022, as shown in Figure 4. Since the spatial distributions at the 24- and 48-month time scales are similar to that at the 12-month time scale, they are not shown. In August 2022, the regional average precipitation anomaly was −68 mm, which was even more severe than the −61 mm precipitation deficit in August 2006. Furthermore, when comparing the 3-month SPEI (Figure 4a and 4g), although the percentage of grids with SPEI <−2 in August 2006 was 25%, which is higher than that in August 2022, the percentages of grids with SPEI less than −1 were around 50% for both cases. Additionally, in August 2022, nearly entire SWC was covered by grid points with SPEI<0, exceeding 75% of the area in August 2006. Overall, if only precipitation or short-term SPEI is considered, the intensities of the two drought events would appear comparable. However, in reality, the CMI reveals a fundamental difference between them. August 2006 experienced a super drought with a CMI value of −1.9, whereas August 2022 did not, with a CMI value of only −0.7. The reason for this difference is that before August 2022, precipitation in SWC had been persistently above normal, maintaining a significantly wet state (Figure 3). By August, although precipitation was significantly below average and short-term droughts covered almost entire SWC (Figure 4g), medium- and long-term droughts had not yet formed (Figures 4h and 4i), so that multiscalar droughts did not superimpose. The frequency distribution in Figure 4k also shows that as the time scale

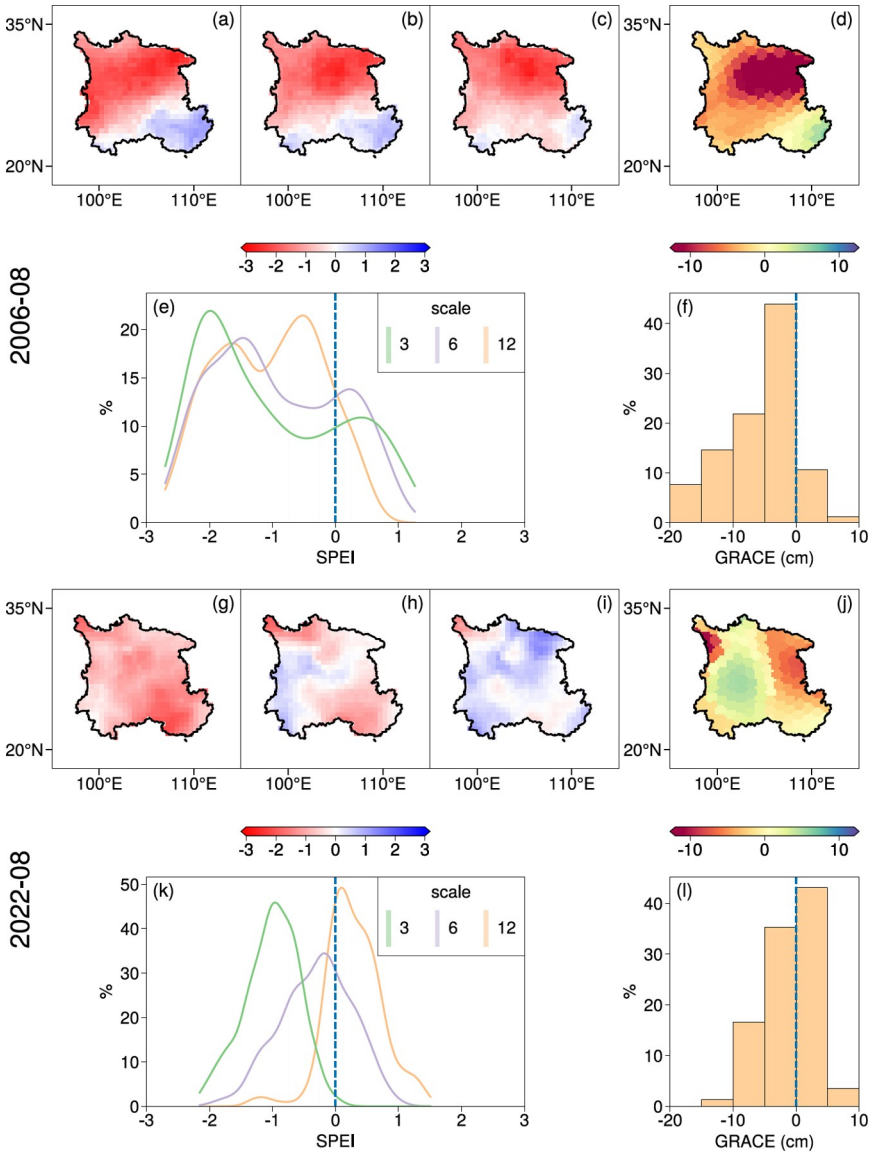

Figure 4 Comparison of drought conditions between August 2006 ((a)–(f)) and August 2022 ((g)–(l)) in SWC. (a)–(f) For August 2006, the spatial distribution of 3-, 6-, and 12-month SPEI ((a)–(c)), the frequency distribution of SPEI (e), the spatial distribution of GRACE terrestrial total water storage anomalies (mm) (d), and the frequency distribution of GRACE terrestrial total water storage anomalies (f). (g)–(l) Same as (a)–(f), but for August 2022.

increases, the probability distribution gradually shifts to the right, i.e., towards the wetter direction, with SPEI values greater than 0 accounting for more than 76% of the regional area at time scales of 12 months and above. In contrast, in August 2006, severe drought conditions prevailed across all time scales spatially (Figure 4a, 4b, and 4c), and the SPEI frequency distributions for all time scales were significantly skewed to the left (Figure 4e). Figure 3 shows that the super drought in August 2006 can be traced back to the frequent seasonal precipitation deficits starting in the autumn of 2003, which led to the establishment and persistence of medium- and long-term hydrological droughts. On this basis, the severe meteorological drought that occurred in the summer of 2006 prompted the simultaneous occurrence and compounding of droughts across all time scales, ultimately resulting in a super drought. Using GRACE satellite data to analyze changes in terrestrial total water storage, it was found that in August 2006, 88% of SWC had negative anomalous water storage, with 22% of the area experiencing a reduction exceeding −10 cm (Figure 4d and 4f). In contrast, in August 2022, 47% of the grids were still in a wet state, with only 1% of the grids experiencing a total water resource deficit greater than −10 cm (Figure 4j and 4l).

The above results clearly demonstrate that the several major drought events that occurred in SWC were caused by the compounding of droughts at different time scales. This once again substantiates the necessity of the super drought concept, emphasizing that only when different types of water resources in a region simultaneously experience extreme states does it constitute a high-impact drought event. It also

verifies that the CMI can effectively integrate multiscalar information and accurately determine the overall severity of regional drought.

5. Analysis of the compounding effects of multiscalar driving variables and circulation anomalies

5.1 Relative contributions and effects of multiscalar precipitation and evaporation

The previous section analyzed the effect of multiscalar drought superposition. This section examines the compounding effects of multiscalar driving variables and circulation anomalies. First, the contributions of precipitation and evaporation are quantitatively attributed, then the roles of multiscalar driving variables in super droughts are assessed, and finally, the climatic causes affecting multiscalar evaporation and precipitation anomalies are investigated.

To quantitatively analyze the contributions of the two factors, precipitation and evaporation, to super drought, experiments were conducted by controlling precipitation and PET using observed values or climatological means. This allows for the quantitative partitioning of the contributions from precipitation, PET, and their combined effects (Yin et al., 2023). The detailed attribution method is provided in Appendix B. Figure 5a presents the contributions of precipitation anomalies, PET anomalies, and their joint effects on the CMI during the months when super droughts occurred in SWC. The results show that the contribution of precipitation ranges from 39% to 71%, with an average of 59%; the contribution of PET ranges from 6% to 48%, with an average of 25%; and the contribution of their joint effects ranges from 1% to 39%, with an average of 16%. If the joint effects are not considered, on average, the contribution of precipitation is 2.4 times that of PET. Thus, precipitation plays a dominant role, while the contribution of evaporation is relatively small. To intuitively explain the conclusion that precipitation contribution dominates super droughts, Figures 5b–5d show the standard deviations of monthly precipitation, PET, and actual evaporation in SWC from 2003 to 2022 to represent the variability characteristics of each variable. The results show that the variability amplitudes of PET and actual evaporation are nearly comparable, with a regional average standard deviation of about 24 mm. However, the standard deviation of precipitation reaches 80 mm, which is

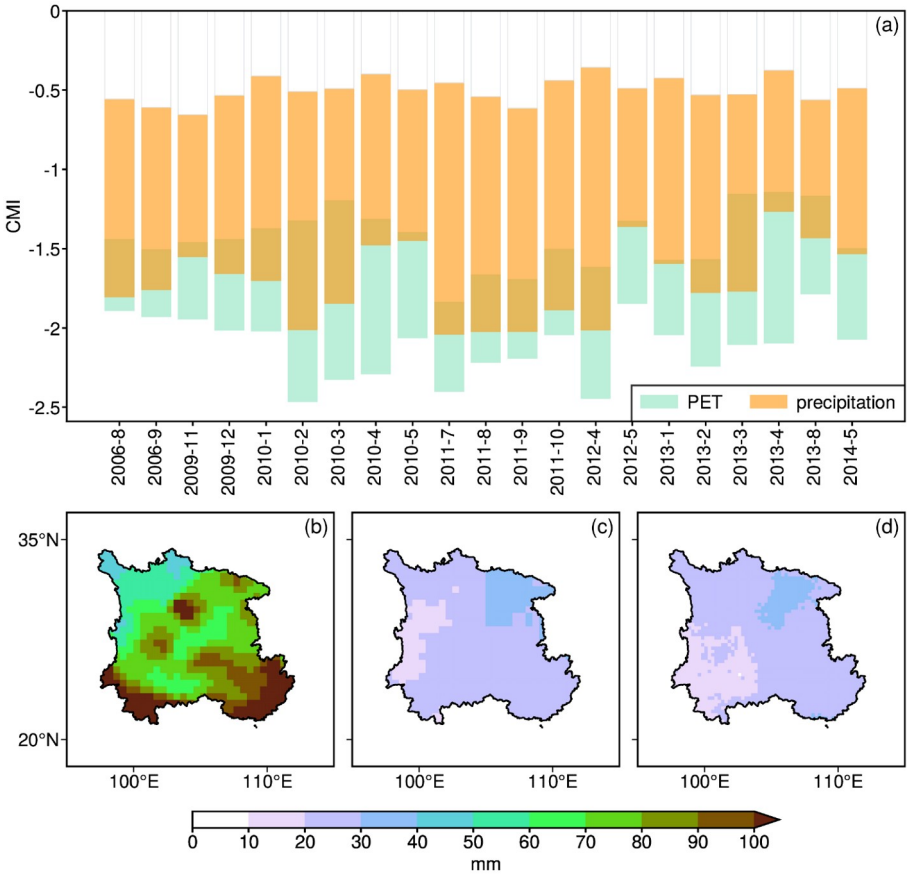

Figure 5 (a) Contributions of precipitation anomalies (orange), PET anomalies (cyan), and their joint effects (brown) to the CMI during the months when super droughts occurred in SWC. The blank part represents the baseline CMI values when both precipitation and PET are set to the climatic means. (b)–(d) Standard deviations (unit: mm) of monthly precipitation, PET, and actual evaporation during 2003–2022.

3.3 times that of evaporation. Since the change in water balance depends on the change in PET minus precipitation (PET–P), the larger range of precipitation variation inevitably leads to a more pronounced change in water balance. Therefore, from the perspective of variability, the dominant contribution of precipitation anomalies to water balance changes, and consequently to super drought events, can be reasonably explained.

Here, it is also necessary to address the following question: Since precipitation contribution is dominant, why do the monthly precipitation anomalies in Figure 2a fail to indicate the occurrence of super droughts? This is mainly due to two reasons. First, there exists a time lag between drought and precipitation anomalies, meaning that precipitation deficits need to accumulate over a period before eventually leading to drought conditions. Second, different types of droughts respond to precipitation anomalies at different time scales. That is, in addition to meteorological droughts at monthly/seasonal scale, agricultural and hydrological droughts require accumulation over longer time scales. This suggests that when analyzing droughts, it is necessary to fully consider their multiscalar evolution characteristics. A significant precipitation deficit in a particular month does not necessarily imply that drought conditions at other medium and long time scales have already developed. According to the definition of super drought, only when droughts at multiple time scales simultaneously reach severe levels does it constitute a true extreme drought event. Therefore, although monthly precipitation anomalies play a dominant role, they are not sufficient to independently indicate super droughts. Rather, the "accumulation" and "compounding" effects across multiple scales need to be considered to accurately reveal the occurrence of super droughts. There is no contradiction between these two aspects.

The following evaluates the effects of multiscalar driving variables on super droughts. Figure 6 presents the changes in PET and precipitation accumulated at the 3-month and 24-month time scales from 1961 to 2022. It should be noted that, to save space, the 3-month and 24-month time scales are used to represent short-term and long-term scales, respectively. As shown in Figures 6b and 6d, the frequent occurrence of super droughts between 2006 and 2014 was primarily determined by the interdecadal anomalies of long-term (24-month) evaporation and precipitation. Specifically, starting from 2003, the 24-month scale evaporation remained at an elevated level until 2017 before returning to normal. During this period, the average positive anomaly of PET reached 57.6 mm, with the maximum positive anomaly as high as 105.6 mm, which was unprecedented since 1961 (Figure 6b). Concurrently, from 2004 onwards, the 24-month precipitation remained persistently low and the overall trend showed a significant decline until it returned to normal levels in 2015, albeit with a brief recovery in between. During this period, the average precipitation deficit reached −96 mm, with a minimum of −336 mm, which was also unprecedented since 1961. Under such an interdecadal background, when significant anomalies emerge at short time scales (e.g., 3 months), the occurrence of super droughts is triggered. The data show that during the super drought events, the 3-month PET increased significantly, with an average increase of 19.8 mm; while the 3-month precipitation decreased significantly, with an average decrease of −60 mm. It should be noted that such short-term anomalies are not uncommon in the historical record; they were merely the necessary conditions for the occurrence of super droughts. What is truly critical is its compounding effect with the interdecadal background.

The above analysis can be summarized as follows. The frequent occurrence of super droughts in SWC is mainly due to the compounding of anomalies in driving variables across multiple time scales. The interdecadal background serves as a necessary condition for shaping the overall pattern of super droughts, while short-term precipitation and evaporation anomalies trigger the outbreak of super droughts, determining the exact occurrence time of super droughts. It is this superposition of climate anomalies across multiple scales that lies at the core of the formation of super droughts.

5.2 Analysis of the main driving factors affecting multiscalar evaporation changes

Next, we analyze the main driving factors affecting multiscalar evaporation changes. The change in evaporation mainly depends on four meteorological elements: temperature, radiation, atmospheric humidity, and wind speed, which influence evaporation intensity through different physical processes. To maintain consistency with the calculation of CRU PET, this study adopts the same Penman-Monteith calculation scheme, with the detailed calculation formulas available in Allen et al. (1998). The main CRU data used include monthly average, maximum, and minimum temperatures, actual vapor pressure, and cloud cover, while wind speed is set as the climatic average value, and cloud cover is used to estimate net radiation. According to the formula, different factors lead to increased PET through different physical processes. On the one hand, an increase in temperature or a decrease in atmospheric humidity directly leads to an increase in the saturation vapor pressure deficit, thereby promoting evaporation. On the other hand, a decrease in cloud cover means an increase in net radiation reaching the surface, providing more energy for evaporation.

To quantitatively distinguish the relative contributions of different factors, we adopt the controlled variable method for analysis. For example, when analyzing the contribution of temperature, we set the temperature to its climatic average, and the difference between the observed PET and the PET

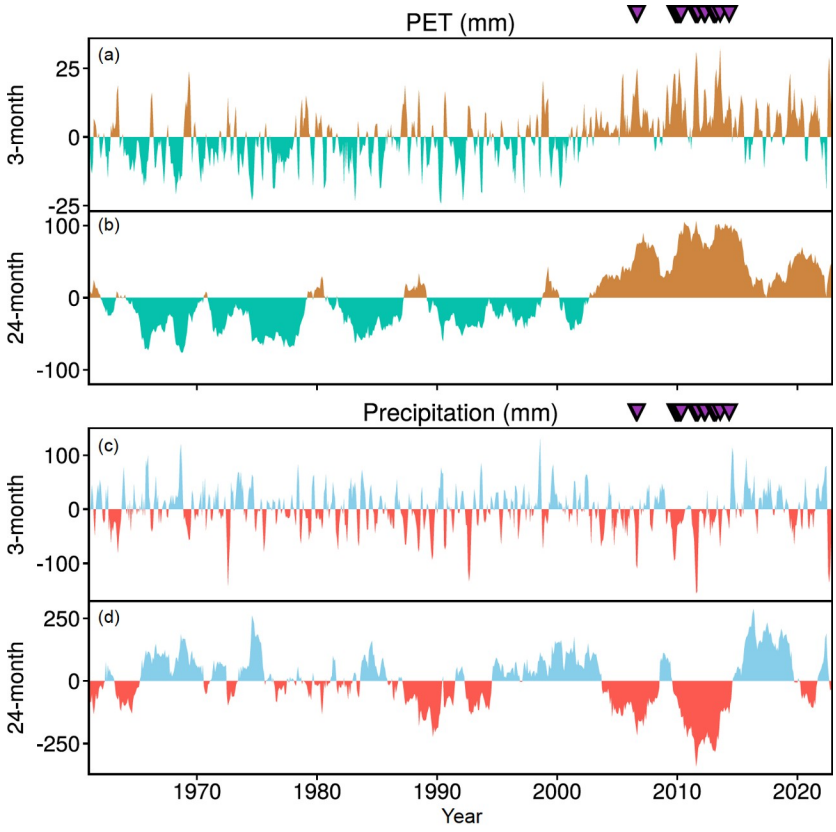

Figure 6 Time series of PET ((a)–(b)) and precipitation ((c)–(d)) anomalies accumulated at 3-month and 24-month time scales from 1961 to 2022.

calculated with a fixed temperature can be approximately attributed to the contribution of temperature changes. Similarly, the contributions of humidity and radiation can also be estimated via similar methods. Through the analysis of several super drought cases, we find that regardless of short-term or long-term time scales, the influence of humidity changes on evaporation is negligible. Temperature increase and radiation increase are the main factors affecting evaporation, with their respective contributions being 41% and 59%, respectively.

By further analyzing the linear trends of temperature and cloud cover data in SWC from 1961 to 2022, it is found that there is a significant increasing trend in temperature during this period, with an average warming rate of 0.015°C year^{-1}, exceeding the 0.001 significance level. This indicates that SWC has experienced significant warming over the past 60 years. However, cloud cover does not show a statistically significant long-term trend. By decomposing the temperature change into long-term trend and interannual variability, the relative contributions of these two components to evaporation are evaluated using the same controlled variable method. The results show that during the periods when super droughts occurred in SWC, the temperature anomalies were caused by both long-term warming trend and interannual fluctuations, each contributing 50%.

In summary, the increase in evaporation when super droughts occurred in SWC is mainly attributed to changes in temperature and radiation, with the contribution rates of these two factors being roughly equal. Further analysis indicates that the long-term warming trend and interannual variability of temperature have equal importance on evaporation, while the effect of radiation mainly originates from interannual fluctuations. In addition, the time scale has little influence on the magnitude of the relevant contribution rates.

5.3 Atmospheric circulation causes of multiscalar precipitation anomalies

Based on the multiscalar processing of atmospheric and oceanic variables described in Section 3.3, we now analyze the atmospheric circulation mechanisms responsible for multiscalar precipitation anomalies. It is well acknowledged that regional precipitation changes are primarily influenced and controlled by two factors: moisture conditions and vertical motion.

To reveal the changes in these two factors at different time scales and their impacts on precipitation, we first draw and analyze Figures 7 and 8. Figure 7 shows the latitude-time cross-sections of moisture flux and divergence anomalies at 3-, 6-, 12-, 24-, and 48-month scales in SWC from 1961 to 2022, while Figure 8 displays the height-time cross-sections of vertical velocity and specific humidity anomalies for the

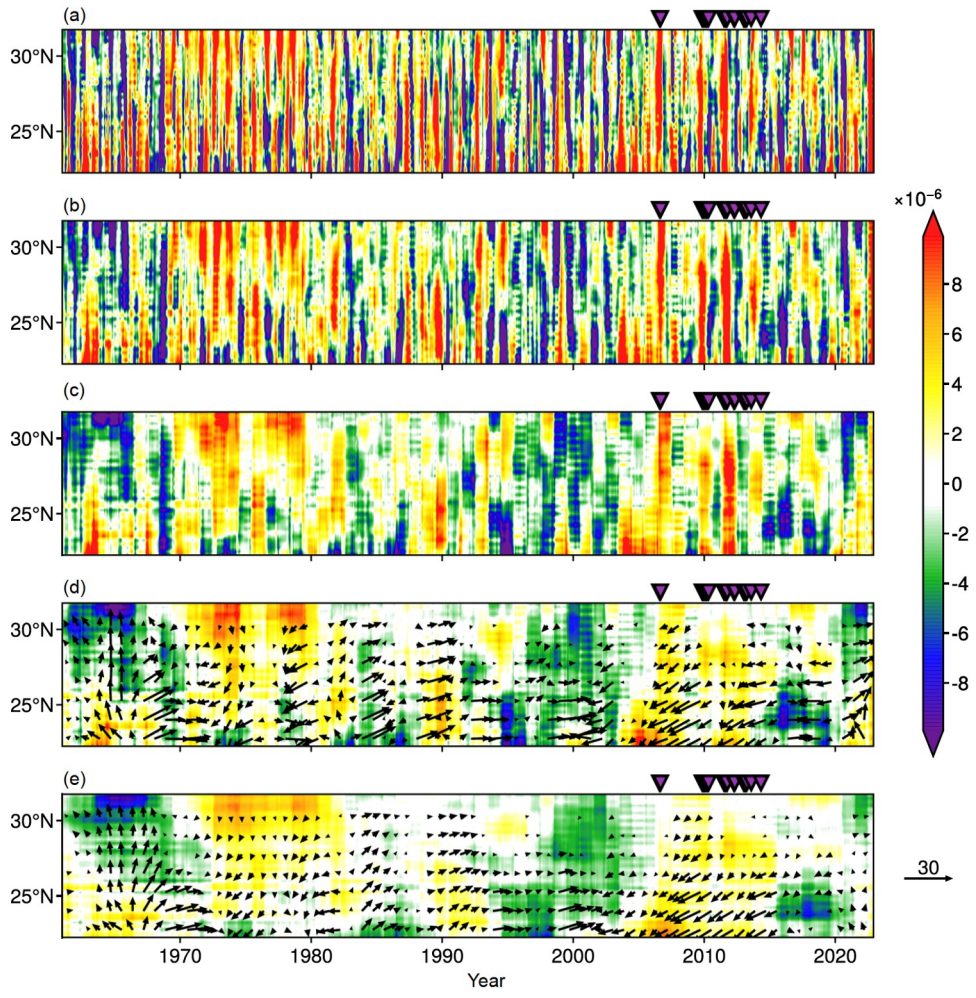

Figure 7 Latitude-time cross-sections of anomalous vertically integrated moisture flux divergence (unit: kg m^{-2} s^{-1}, shaded) at 3-, 6-, 12-, 24-, and 48-month ((a)–(e)) time scales over SWC from 1961 to 2022. The corresponding vertically integrated moisture flux anomalies (unit: kg m^{-1} s^{-1}, vectors) are also overlaid at 24- and 48-month time scales ((d), (e)).

corresponding time scales. These two sets of figures show that as the time scale increases, the changes in variables such as moisture flux divergence, vertical velocity, and specific humidity become more gradual, with positive and negative anomalies persisting for longer durations. At the short 3-month time scale, regional precipitation anomalies show significant negative correlations with moisture flux divergence and 500 hPa vertical velocity anomalies, with correlation coefficients of −0.58 and −0.8, respectively, both passing the 0.001 significance level test. This indicates that short-term precipitation changes in SWC are mainly controlled by anomalies in moisture conditions and convective activity, with the latter having a greater influence. On long time scales, both moisture and vertical motion exhibit obvious interdecadal variations, forming relatively stable wet or dry background conditions. For instance, around 1970, 2000, and 2015–2020, there was a significant enhancement of southerly moisture transport, a substantial increase in moisture content, and an accompanying rising airflow, corresponding to increased precipitation during these periods. In contrast, during the periods around 1980 and 2006–2014, prevailing northeasterly wind anomalies hindered the transport of moisture from the oceans to the south of SWC, leading to decreased moisture content and pronounced subsidence, which suppressed convective activity and precipitation. During the period from 2006 to 2014, when super droughts frequently occurred, the most significant northeasterly moisture transport anomalies, as well as persistent moisture divergence and sinking airflow throughout the entire layer, formed an unfavorable circulation background for precipitation on long time scales. On this basis, the superposition of short-term circulation anomalies led to the occurrence of super droughts.

Next, we further analyze the spatial patterns of circulation anomalies over SWC and East Asia at different time scales during the occurrence of super droughts, as shown in Figure 9. Here, we select 3-month and 24-month time scales to represent short-term and long-term droughts, respectively, and then show the joint distributions of regional vertical motion and precipitable water, as well as the spatial patterns

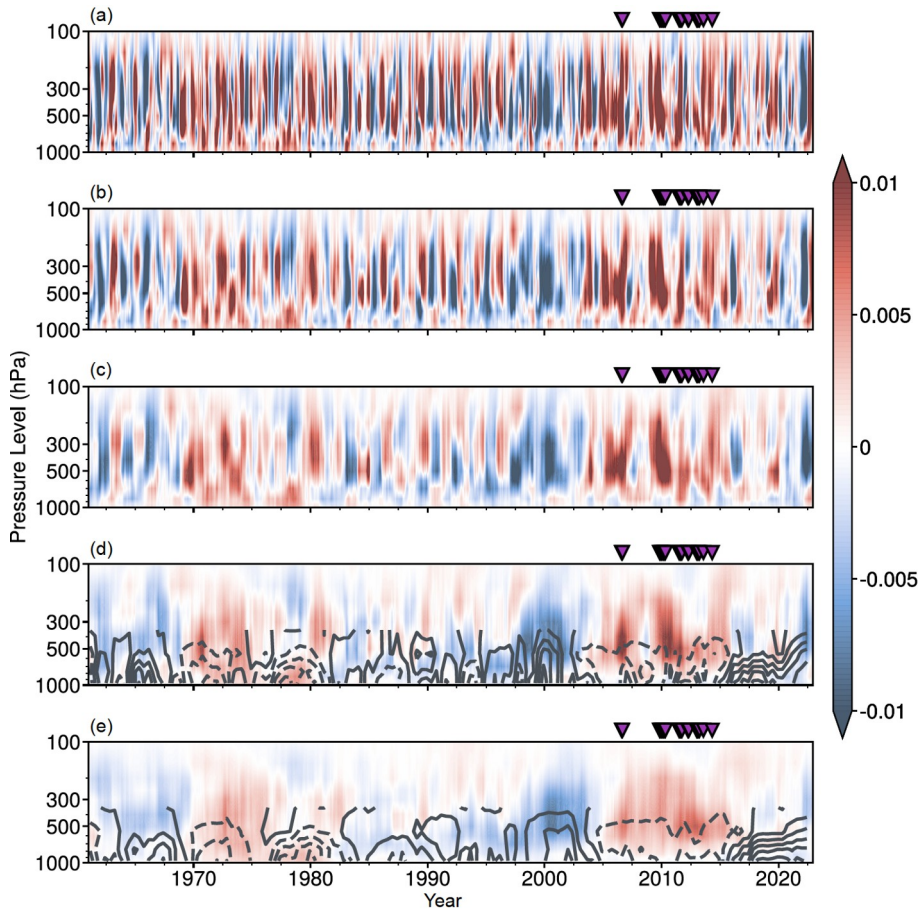

Figure 8 Height-time cross-sections of vertical velocity anomalies (unit: Pa s^{-1}, shaded) over SWC at 3-, 6-, 12-, 24-, and 48-month ((a)–(e)) time scales from 1961 to 2022. The corresponding specific humidity anomalies (unit: kg kg^{-1}, contours; solid lines for positive and dashed lines for negative) at 24-month and 48-month time scales are also overlaid ((d), (e)).

of large-scale circulation anomalies. The choice for these two time scales is representative: on the one hand, the 3-month and 24-month time scales can reflect the short-term and long-term effects of drought; on the other hand, the relatively low correlation between the patterns at these two time scales implies stronger independence, warranting separate discussions. Therefore, selecting these two most representative time scales for analysis can concisely summarize the causal mechanisms involved. Of course, for the sake of completeness, we also provide composite maps of moisture flux and vertical velocity anomalies for all five typical time scales in Appendix C (Figures S2 and S3). Figures S2 and S3 show that the patterns at the 3-month and 6-month time scales exhibit similarities, while the patterns at the 24-month time scale are more akin to those at the 12-month and 48-month time scales, further justifying the selection of the 3-month and 24-month scales for analysis. Finally, it is particularly important to emphasize that although Figure 9 focuses on analyzing the anomalous circulation characteristics at the 3-month and 24-month time scales, the calculation of the CMI is not solely based on these two time scales but rather comprehensively considers the contributions of all 5 typical time scales.

By statistically analyzing the joint distributions of precipitable water and 500 hPa vertical velocity over SWC at 3-month short-term and 24-month long-term scales, it is found that when super droughts occur, the vertical velocities at both time scales correspond to significant positive anomalies, while the precipitable water exhibits negative anomalies (Figures 9a and 9b). This indicates that super droughts correspond to the multiscalar extreme anomalies in both the dynamic and moisture conditions within the region. Moreover, the positive anomaly of vertical velocity is more significant, suggesting that the anomaly of dynamic conditions plays a dominant role in the formation of super droughts in SWC. Building upon the local analysis, we further examine the large-scale circulation characteristics through composite analysis. Here, we composite all the months when super drought events occurred, as marked in Figure 5a. Additionally, for the 3-month time scale, the traditional *t*-test method is used for significance testing of the composite fields, while for the 24-month time scale, which exhibits substantial autocorrelation, the block bootstrap method is adopted. This method is a nonparametric resampling tech-

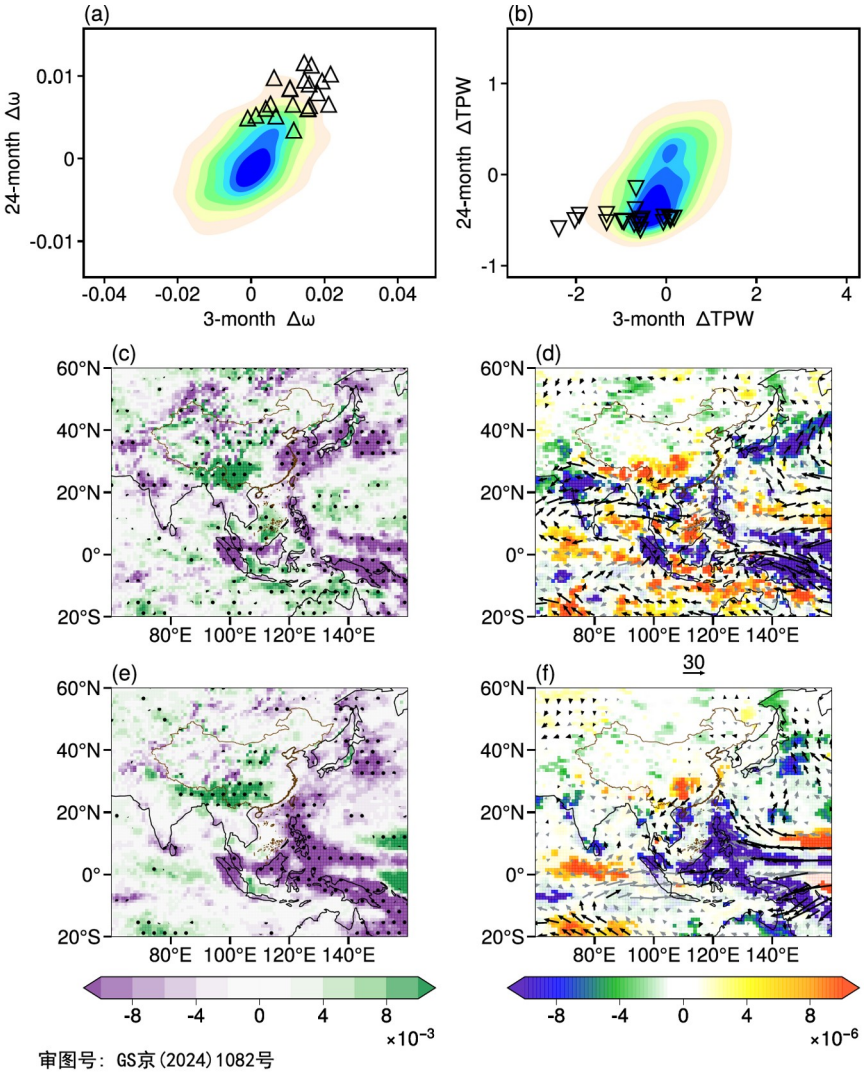

Figure 9 (a) Joint density distribution (shaded) of regionally averaged 500 hPa vertical velocity anomalies (unit: Pa s^{-1}) at 3-month (*x*-axis) and 24-month (*y*-axis) time scales over SWC, with values during super drought months marked by triangles. (b) Same as (a), but for total column precipitable water anomalies (unit: kg m^{-2}). (c) Composite spatial distribution of 500 hPa vertical velocity at 3-month time scale during super drought months. (d) Composite spatial distribution of vertically integrated moisture flux (unit: kg m^{-1} s^{-1}, arrows) and moisture flux divergence anomalies (unit: kg m^{-2} s^{-1}, shaded) at 3-month time scale during super droughts months. (e), (f) same as (c), (d), but for 24-month time scale. For the spatial distribution of vertical velocity ((c), (e)), the dotted areas pass the 0.1 significance test. For the moisture flux vectors ((d), (f)), vectors passing or failing the 0.1 significance level are shown in black or gray, respectively, and moisture flux divergence shaded areas failing the 0.1 significance level have 90% transparency.

nique suitable for time series data with autocorrelation, which preserves the autocorrelation structure of the original data by repeatedly sampling continuous data blocks (Lahiri, 2003). The number of repeated samples is set to 10,000 here. By compositing the 500 hPa vertical velocity and moisture fields over East Asia during super droughts at short-term and long-term scales, the similarities and differences in the spatial patterns of circulation anomalies at different scales are compared, as shown in Figures 9c–9f. The results show that in terms of the vertical velocity, the anomalous spatial patterns at short-term and long-term scales have a certain degree of similarity, both corresponding to a significant sinking anomaly center over SWC. However, at the long-term scale, the associated enhanced convective region is mainly located in the Indo-Pacific warm pool and the tropical northwestern Pacific, while at the short-term scale, it corresponds to a significant ascending anomaly over the Yangtze River basin to Japan. Regarding the moisture flux, both short-term and long-term scales feature moisture flux divergence and northeasterly wind anomalies over SWC. However, at the short-term scale, the anomalous cyclone is mainly confined to the northern part of the South China Sea, whereas at the long-term scale, the corresponding anomalous cyclone extends over the entire South China Sea and equatorial region. Moreover, at the short-term scale, the region to the south of the Tibetan Plateau extending to the Bay of Bengal is controlled by easterly wind anomalies, which are not conducive to moisture transport from the Bay of Bengal, but at the long-

term scale, there is no significant anomaly in the northern Indian Ocean region. Overall, the occurrence of super droughts corresponds to the compounding of circulation anomalies at short-term and long-term scales, leading to the formation of regional extreme drought events.

This study also analyzes the circulation systems affecting short-term (3-month) precipitation anomalies in SWC across different seasons. Using the regression analysis method, the characteristics of moisture transport anomalies associated with SWC precipitation anomalies in spring, summer, autumn, and winter are analyzed (figures not shown). The results show that the main circulation features are consistent with the aforementioned composite analysis results, corresponding to the cyclonic anomaly over the South China Sea and the easterly wind anomalies over the Bay of Bengal. Both of these anomalies would inhibit the transport of water vapor from the tropical ocean to SWC, which is not conducive to the generation of precipitation. However, the relative influence of these two moisture transport systems varies in different seasons: in summer and autumn, the South China Sea cyclonic anomaly and the Bay of Bengal easterly wind anomaly exert comparable influences on SWC precipitation; in spring, the influence of anomalous flows controlling moisture supply from the northern Indian Ocean is more significant; while in winter, due to the relatively small precipitation anomalies, it can be disregarded. As this study primarily focuses on the compounding effect of drought signals at different time scales, and there is a large body of literature exploring the causes of short-term drought events, we will not elaborate further here.

Next, we focus on analyzing the possible formation mechanism of the interdecadal background of persistently reduced cross-seasonal precipitation in SWC during the period 2003–2014. It is worth noting that although some studies have analyzed the interdecadal variations of precipitation in SWC, most of them have concentrated on the changes in a particular season. In fact, the interdecadal decrease in precipitation in only one season is not sufficient to form the long-term drought background required for super droughts, because changes in other seasons may offset the anomalies in that season. The long-term precipitation changes concerned in this study reflect the cumulative effect of precipitation across seasons, thus representing a comprehensive influence of different seasons. The formation of this interdecadal background provided important preconditions for the subsequent superposition of short-term circulation anomalies, leading to the emergence of super drought events.

Figure 10 shows the three-dimensional characteristics of the large-scale SST and circulation anomalies averaged over the period from January 2003 to December 2014. The lower layer presents the anomalous distribution of internal SST variability and the corresponding circulation anomalies at 850 hPa, while the upper layer shows the divergent wind anomalies at 200 hPa and divergence. In between these two levels, a slanted cross-section describes the vertical structure of the wind field from (30°N, 100°E) to (0°, 130°E). The vertical velocity is magnified by 100 times to enhance visibility. The external forcing signal of SST is removed following the method of Dai et al. (2015). Specifically, the ensemble mean of the global mean SST sequence from 36 CMIP6 models (Appendix D) is treated as the external forcing signal, and the observed SST anomaly time series at each grid point is regressed onto the ensemble mean global mean SST changes, with the regression field considered as the change caused by external forcing and the residual part as internal variability. From the three-dimensional structure, two important remote forcing systems controlling the interdecadal drought background in SWC can be clearly identified: the negative phase of the PDO in the North Pacific and the enhanced convection over the western Pacific warm pool. First, regarding the influence of the negative PDO phase, there is a positive SST anomaly zone in the mid-high latitudes of the North Pacific, while negative SST anomalies prevail in the region extending from the west coast of North America to the central-eastern equatorial Pacific. The former triggers an anomalous anticyclonic circulation, with the associated northeasterly winds extending to the Southeast Asian region on its southwestern flank, hindering moisture transport towards SWC and suppressing precipitation. It is noteworthy that the observed circulation anomaly pattern associated with this negative PDO phase is basically consistent with the response simulated by an atmospheric model driven by PDO cold events, as reported in previous studies (Yang et al., 2017). To reflect the long-term evolution of the PDO, Figure 11b presents the time series of the PDO index from 1961 to 2022. It can be seen that after 2003, the PDO index remained negative and reached its lowest value in 60 years, consistent with the period of super drought background in SWC. However, statistical analysis shows that there is no obvious correlation between the PDO index and the 24-month precipitation in SWC when considering the entire period. This suggests that the factors influencing the interdecadal variation of precipitation in SWC are relatively complex, and the role played by the negative PDO phase during 2003–2014 was more prominent, while the interdecadal background mechanisms in other periods remain to be further analyzed.

Next, we examine the role of the warm pool in the tropical western Pacific. From the internal SST pattern after removing the external forcing (shown in the lower level of Figure 10), it can be seen that when the PDO is in a negative phase, although the warm pool in the western Pacific corresponds to a positive SST anomaly, its magnitude is not significant. This suggests that the enhanced convection in this region may be the result of external forcing rather than internal climate variability. Figure 11a presents the linear trend of annual

mean SST over the past 60 years. It can be observed that the most significant warming occurs over the warm pool in the western Pacific, while the SST trend in the tropical central-eastern Pacific is weaker. The abnormal warming in the western Pacific warm pool triggers an enhanced convective response over the region, which excites an anomalous cyclonic circulation to its northwest according to the Gill mode response. Consequently, northeasterly wind anomalies are formed over SWC, which is unfavorable for moisture transport. Concurrently, the persistent strong ascending motion over the warm pool diverges aloft, with one branch of the airflow tending towards SWC, forming anomalous sub-

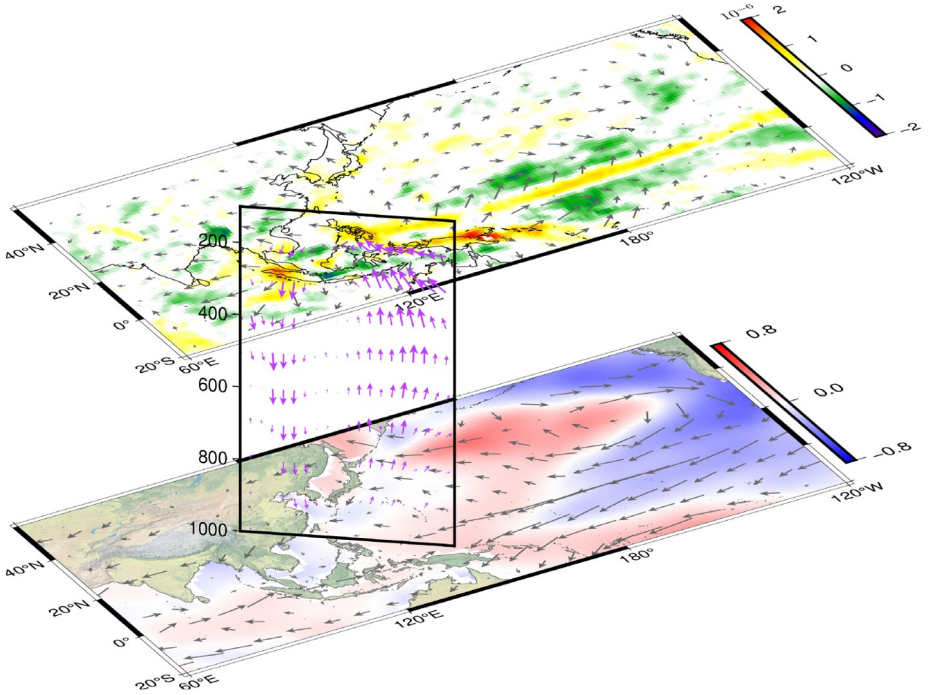

Figure 10 Three-dimensional features averaged over the period from January 2003 to December 2014 at the 24-month time scale. The lower layer shows the distribution of SST anomalies after removing the external forcing signal (unit: °C) and the 850 hPa wind anomalies (unit: m s^{-1}), while the upper layer shows the 200 hPa divergent wind (unit: m s^{-1}) and divergence anomalies (unit: s^{-1}). The slanted cross-section along (30°N, 100°E) to (0°, 130°E) between the lower and upper layers depicts the vertical wind structure, with the vertical velocity multiplied by 100.

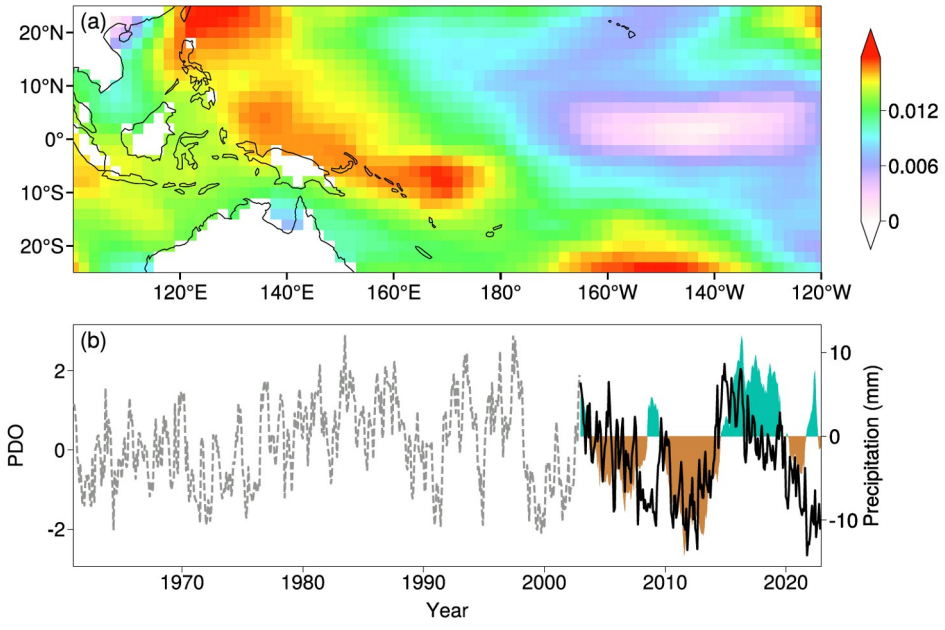

Figure 11 (a) Linear trend of annual mean SST (unit: °C $year^{-1}$) from 1961 to 2022. (b) Time series of the PDO index (left *y*-axis, line chart) and 24-month precipitation anomalies (right *y*-axis, area chart) over SWC from 1961 to 2022.

sidence there.

Therefore, the combined effect of these two remote forcings, the negative PDO phase and the enhanced convection over the western Pacific warm pool, formed the key elements in the long-term climatic background state that are unfavorable for precipitation in SWC. This provided an important precondition for the subsequent superposition of short-term extreme precipitation deficits to trigger super drought events.

6. Conclusions

This study comprehensively analyzes the characteristics of super droughts in SWC from 1961 to 2022 based on the Comprehensive Multiscalar Index (CMI), and reveals the compounding effects of droughts across multiple time scales as well as the associated atmospheric circulation driving mechanisms. The main conclusions are as follows:

Super drought corresponds to the superposition of extreme droughts at different time scales. By contrasting typical drought cases in 2006 and 2022, it is confirmed that comprehensive consideration of multiscalar drought information is crucial, emphasizing that the essence of extreme drought events is the joint shortage of water resources across different types.

Multiple super drought events occurred frequently in SWC during 2006–2014. Among them, the interdecadal background of enhanced evaporation and precipitation deficit at long time scales is a necessary condition for shaping the overall pattern of super droughts. The precipitation and evaporation anomalies at short time scales triggered the outbreak of super droughts, determining the exact occurrence time, including August–September 2006, November 2009 to May 2010, July–October 2011, April–May 2012, and January–April 2013.

Quantitative analysis reveals that precipitation plays a dominant role, while the contribution of evaporation is relatively small, with the former being 2.4 times that of the latter. The increase in evaporation is mainly attributed to changes in temperature and radiation, with roughly equal contributions from these two factors.

Regarding the circulation mechanisms affecting multiscalar precipitation, the composite analysis of super drought cases shows that the anomalous spatial patterns at short-term and long-term scales are similar. They are characterized by the cyclonic circulation over the South China Sea, and the northeasterly wind anomalies along with the sinking anomaly center over SWC, thereby suppressing regional precipitation generation through the superposition of anomalies across different time scales.

During 2006–2014, SWC experienced the most significant northeasterly moisture transport anomalies, as well as moisture divergence and sinking features. This is mainly due to the extremely negative phase of the PDO and the abnormal warming in the western Pacific warm pool after 2003. These two remote forcings jointly formed a key climatic background unfavorable for precipitation in SWC on long time scales, providing an important precondition that allowed the superposition of short-term extreme precipitation deficits to trigger super drought events.

The main dynamic processes causing the persistent reduction of cross-seasonal precipitation in SWC due to the negative PDO phase and the warming in the western Pacific warm pool are as follows. On the one hand, the negative PDO phase triggers an anomalous anticyclonic circulation over the North Pacific, with the associated northeasterly winds on its southwestern flank extending to the Southeast Asian region, which hinders moisture transport. On the other hand, the warming in the warm pool region induces anomalous cyclonic circulation to its northwest, also forming northeasterly wind anomalies over SWC. Meanwhile, the ascending motion over the warm pool region diverges aloft and converges over SWC, leading to compensating sinking motion there.

In summary, these research findings emphasize the pivotal role of the compounding effects of climatic anomalies at different time scales in the formation of super droughts, which provides important implications for deepening the understanding the nature and causes of regional-scale extreme drought events.

Acknowledgements *This work was supported by the National Natural Science Foundation of China (Grant Nos. 42175041 & 42230605), the International Partnership Program of Chinese Academy of Sciences for Future Network (Grant No. 060GJHZ2022104FN), the Youth Program of the Institute of Atmospheric Physics, Chinese Academy of Sciences during the 14th Five-Year Plan Period, and the Open Research Fund of Heavy Rain and Drought-Flood Disasters in Plateau and Basin Key Laboratory of Sichuan Province (Grant No. SZKT202204).*

Conflict of interest The authors declare that there are no conflicts of interest.

References

Allen RG, Pereira LS, Raes D, Smith M. 1998. Crop evapotranspiration–guidelines for computing crop water requirements. FAO Irrigation and drainage paper 56, Rome, http://www.fao.org/docrep/X0490E/X0490E00.htm

Chen W, Zhang R, Wu R, Wen Z, Zhou L, Wang L, Hu P, Ma T, Piao J, Song L, Wang Z, Li J, Gong H, Huangfu J, Liu Y. 2023. Recent advances in understanding multi-scale climate variability of the Asian monsoon. Adv Atmos Sci, 40: 1429–1456

Chen W, Piao J, Chen S, Wang L, Zhao W, Wang Z, Wang Q. 2024. Multi-Scale variations and future projections of dry-wet conditions over the monsoon transitional zone in East Asia: A review. Fundam Res, http://doi.org/10.1016/j.fmre.2024.01.023

Dai A, Fyfe J C, Xie S P, Dai X. 2015. Decadal modulation of global surface temperature by internal climate variability. Nat Clim Change, 5: 555–559

Dong Z, Gui S, Yang R, Cheng J, Yang H, Ma J. 2023. Interdecadal

variation of precipitation over Yunnan, China in summer and its possible causes. Front Environ Sci, 11: 1281202
Duan H, Wang S, Feng J. 2011. The drought in China in summer 2011 and its impacts and causes (in Chinese). J Arid Meteor, 29: 392–400
Hao S, Li J, Mao J. 2022. Interannual relationship between summer North Atlantic Oscillation and subsequent november precipitation anomalies over Yunnan in Southwest China. J Meteorol Res, 36: 718–732
Harris I, Osborn T J, Jones P, Lister D. 2020. Version 4 of the CRU TS monthly high-resolution gridded multivariate climate dataset. Sci Data, 7: 109
Hersbach H, Bell B, Berrisford P, Hirahara S, Horányi A, Muñoz-Sabater J, Nicolas J, Peubey C, Radu R, Schepers D, Simmons A, Soci C, Abdalla S, Abellan X, Balsamo G, Bechtold P, Biavati G, Bidlot J, Bonavita M, De Chiara G, Dahlgren P, Dee D, Diamantakis M, Dragani R, Flemming J, Forbes R, Fuentes M, Geer A, Haimberger L, Healy S, Hogan R J, Hólm E, Janisková M, Keeley S, Laloyaux P, Lopez P, Lupu C, Radnoti G, de Rosnay P, Rozum I, Vamborg F, Villaume S, Thépaut J. 2020. The ERA5 global reanalysis. Quart J R Meteorol Soc, 146: 1999–2049
Hu X, Xu P, Ning G, Wang S, Shang K. 2015. Causes of continuous drought in Southwest China from autumn of 2012 to spring of 2013 (in Chinese). J Desert Res, 35: 763–773
Huang B, Thorne P W, Banzon V F, Boyer T, Chepurin G, Lawrimore J H, Menne M J, Smith T M, Vose R S, Zhang H M. 2017. Extended reconstructed sea surface temperature, Version 5 (ERSSTv5): Upgrades, validations, and intercomparisons. J Clim, 30: 8179–8205
Huang R, Liu Y, Wang L, Wang L. 2012. Analyses of the causes of severe drought occurring in Southwest China from the fall of 2009 to the spring of 2010 (in Chinese). Chin J Atmosph Sci, 36: 443–457
Huo F, Jiang Z, Ma H, Li Z, Li Y. 2021. Reduction in autumn precipitation over Southwest China by anthropogenic aerosol emissions from eastern China. Atmos Res, 257: 105627
Jia X J, Gu Q, Qian Q F, Wu R. 2021. Wet-to-dry climate shift of the Sichuan Basin during 1961–2010. Clim Dyn, 57: 671–685
Jiang X, Shu J, Wang X, Huang X, Wu Q. 2017. The Roles of convection over the western maritime continent and the Philippine Sea in interannual variability of summer rainfall over Southwest China. J Hydromet, 18: 2043–2056
Lahiri SN. 2003. Resampling methods for dependent data. Springer Science & Business Media
Leng X, Liu X, Gao Y, Liu Y, Yang Q, Sun G, Peng Y, Huang Y. 2020. Drought assessment of southwestern China based on HadGEM2-ES model under representative concentration pathway 4.5 scenario. Nat Hazard, 102: 307–334
Li Y, Xu H, Liu D. 2011. Features of the extremely severe drought in the east of Southwest China and anomalies of atmospheric circulation in summer 2006. Acta Meteorol Sin, 25: 176–187
Liu M, Xu X, Sun A Y, Wang K. 2017. Decreasing spatial variability of drought in southwest China during 1959–2013. Intl J Clim, 37: 4610–4619
Martens B, Miralles D G, Lievens H, van der Schalie R, de Jeu R A M, Fernández-Prieto D, Beck H E, Dorigo W A, Verhoest N E C. 2017. GLEAM v3: Satellite-based land evaporation and root-zone soil moisture. Geosci Model Dev, 10: 1903–1925
Miralles D G, Holmes T R H, De Jeu R A M, Gash J H, Meesters A G C A, Dolman A J. 2011. Global land-surface evaporation estimated from satellite-based observations. Hydrol Earth Syst Sci, 15: 453–469
Save H, Bettadpur S, Tapley B D. 2016. High-resolution CSR GRACE RL05 mascons. J Geophys Res-Solid Earth, 121: 7547–7569
Sun S, Li Q, Li J, Wang G, Zhou S, Chai R, Hua W, Deng P, Wang J, Lou W. 2019. Revisiting the evolution of the 2009–2011 meteorological drought over Southwest China. J Hydrol, 568: 385–402
Tan H, Cai R, Chen J, Huang R. 2017. Decadal winter drought in Southwest China since the late 1990s and its atmospheric teleconnection. Int J Clim, 37: 455–467
Tapley B D, Watkins M M, Flechtner F, Reigber C, Bettadpur S, Rodell M, Sasgen I, Famiglietti J S, Landerer F W, Chambers D P, Reager J T, Gardner A S, Save H, Ivins E R, Swenson S C, Boening C, Dahle C, Wiese D N, Dobslaw H, Tamisiea M E, Velicogna I. 2019. Contributions of GRACE to understanding climate change. Nat Clim Chang, 9: 358–369
Tao W, Huang G, Wang P, Wang Y, Gong H, Dong D. 2023. The onset and cessation of rainy season over the Hengduan Mountains. Clim Dyn, 61: 4773–4791
Vicente-Serrano S M, Beguería S, López-Moreno J I. 2010. A multiscalar drought index sensitive to global warming: The standardized precipitation evapotranspiration index. J Clim, 23: 1696–1718
Wang L, Chen W. 2012. Characteristics of multi-timescale variabilities of the drought over last 100 years in Southwest China (in Chinese). Adv Meteor Sci Tech, 2: 21–26
Wang L, Chen W, Zhou W. 2014. Assessment of future drought in Southwest China based on CMIP5 multimodel projections. Adv Atmos Sci, 31: 1035–1050
Wang L, Chen W, Zhou W, Huang G. 2015a. Drought in Southwest China: A review. Atmos Oceanic Sci Lett, 8: 339–344
Wang L, Chen W, Zhou W, Huang G. 2015b. Teleconnected influence of tropical Northwest Pacific sea surface temperature on interannual variability of autumn precipitation in Southwest China. Clim Dyn, 45: 2527–2539
Wang L, Chen W, Zhou W, Huang G. 2016. Understanding and detecting super-extreme droughts in Southwest China through an integrated approach and index. Quart J R Meteorol Soc, 142: 529–535
Wang L, Huang G, Chen W, Zhou W, Wang W. 2018. Wet-to-dry shift over Southwest China in 1994 tied to the warming of tropical warm pool. Clim Dyn, 51: 3111–3123
Wang L, Chen W, Fu Q, Huang G, Wang Q, Chotamonsak C, Limsakul A. 2022. Super droughts over East Asia since 1960 under the impacts of global warming and decadal variability. Intl J Clim, 42: 4508–4521
Wang S, Huang J, Yuan X. 2021. Attribution of 2019 extreme spring-early summer hot drought over Yunnan in Southwestern China. Bull Am Meteorol Soc, 102: S91–S96
Wang L, Huang G, Chen W, Wang T. 2023. Super drought under global warming: Concept, monitoring index, and validation. Bull Am Meteorol Soc, 104: E943–E969
Wu C, Li Q, Dong L, Yan H, Wang D, Sun X. 2023. Rainy season onset date in Southwest China and the related atmospheric circulations. Atmos Res, 298: 107127
Yang Q, Ma Z, Fan X, Yang Z L, Xu Z, Wu P. 2017. Decadal modulation of precipitation patterns over Eastern China by sea surface temperature anomalies. J Clim, 30: 7017–7033
Yin Z, Yang S, Wei W. 2023. Quantitative attribution of vertical motions responsible for the early spring drought conditions over southeastern China. Clim Dyn, 61: 2655–2672
Zhang C. 2020. Moisture sources for precipitation in Southwest China in summer and the changes during the extreme droughts of 2006 and 2011. J Hydrol, 591: 125333
Zhang J, Wu R, Jia X, Zhang Y. 2022. Contribution of precipitation and temperature to multiscale drought variations over Asia: Dependence on the time scale. Intl J Clim, 42: 8804–8821
Zhang L, Sun W. 2022. Progress and prospect of GRACE Mascon product and its application (in Chinese). Rev Geophys Planet Phys, 53: 35–52
Zhang Q, Yao Y, Li Y, Huang J, Ma Z, Wang Z, Wang S, Wang Y, Zhang Y. 2020. Progress and prospect on the study of causes and variation regularity of droughts in China (in Chinese). Acta Meteorol Sin, 78: 500–521
Zhang Q, Li D, Yao Y, Wang Z, Wang Y, Wang J, Wang J, Wang S, Yue P, Wang H, Han L, Si D, Li Q, Zeng G, Wang H. 2024. Research progress and prospect of drought formation mechanism, prediction theory and its disaster risk characteristics (in Chinese). Acta Meteorol Sin, 82: 1–21
Zhang Y, Wu R. 2021. Asian meteorological droughts on three time scales and different roles of sea surface temperature and soil moisture. Intl J Clim, 41: 6047–6064

(Editorial handling: Zhaoxin LI)